PERGAMON

International Journal of Heat and Mass Transfer 41 (1998) 3055–3073

International Journal of HEAT and MASS TRANSFER

Natural convection in a narrow horizontal cylindrical annulus: $Pr \leqslant 0.3$

Joo-Sik Yoo*

Department of Mechanical Engineering Education, Andong National University, 388 Songchun-dong, Andong, Kyungpuk, 760-749, Korea

Received 24 July 1997; in final form 14 January 1998

Abstract

Natural convection in a narrow horizontal cylindrical annulus is numerically investigated for fluids of $Pr \leqslant 0.3$. For $Pr \leqslant 0.2$, hydrodynamic instability induces steady or oscillatory flows consisting of multiple like-rotating cells. For $Pr = 0.3$, thermal instability creates a counter-rotating cell on the top of annulus. For a fluid of $Pr \approx 0$, the multiple cells are distributed uniformly in the lower and upper parts of annulus. As Pr is increased, the cells are shifted upwards. The like-rotating cells drift downward, as time goes on, and the speed of travel increases with increase of Pr. For $Pr = 0.3$, the oscillatory flows after secondary instability consist of multiple like-rotating cells in the vertical section of annulus and one or more counter-rotating cells on the top part, and multiple oscillatory flows are found.

Key words: Natural convection; Transition; Multicellular flow; Multiple oscillatory flows.

Nomenclature

D_i diameter of inner cylinder
$\check{e}_r$, $\check{e}_\phi$ unit vectors in the radial and angular directions, respectively
Gr Grashof number based on the gap width, $\alpha g(T_i - T_o)L^3/\nu^2$
Gr_c critical Grashof number at which instability of conduction regime occurs
g acceleration of gravity
J Jacobian
L gap width of the annulus, $R_o - R_i$
$N(t)$ number of points ϕ at which $u(r_c, \phi-, t) > 0$ and $u(r_c, \phi+, t) < 0$
Nu_{cond} Nusselt number of pure conduction state
Nu_i, Nu_o local Nusselt numbers at the inner and outer cylinders, respectively
$\overline{Nu}_i$, $\overline{Nu}_o$ mean Nusselt numbers at the inner and outer cylinders, respectively
$\overline{Nu}$ overall Nusselt number, $(\overline{Nu}_i + \overline{Nu}_o)/2$
$\overline{Nu}_{time}$ time-averaged overall Nusselt number
P period of oscillation
p dimensionless pressure
Pr Prandtl number, ν/χ
Ra Rayleigh number, $Pr\,Gr$
R_i, R_o radii of the inner and outer cylinders, respectively
r dimensionless radial coordinate
r_i, r_o dimensionless radii of the inner and outer cylinders, respectively
r_c radial coordinate of the center of annular gap, $(r_i + r_o)/2$
t dimensionless time
T_i, T_o temperatures at the inner and outer cylinders, respectively
$\vec{u}$ dimensionless velocity vector
u, v dimensionless velocity components in the radial and angular directions, respectively
$u(t)$ instantaneous radial velocity at $(r_c, \pi/2)$, $u(r_c, \pi/2, t)$.

Greek symbols

α coefficient of thermal expansion
η stretched coordinate in the radial direction
θ dimensionless temperature
χ thermal diffusivity

* Corresponding author.

0017–9310/98 $19.00
PII: S0017-9310(98)00051-9

ν kinematic viscosity
ρ_0 mean density
ϕ angular coordinate
Ψ dimensionless streamfunction
ω dimensionless vorticity.

1. Introduction

Natural convection in a horizontal concentric cylindrical annulus kept at constant surface temperatures has received much attention because of the theoretical interest and its wide engineering applications such as thermal energy storage systems, cooling of electronic components and transmission cables. Comprehensive reviews were presented by Gebhart et al. [1].

The flow features of a fluid with high Prandtl number (of order 1 or larger) have been disclosed experimentally and numerically. Kuehn and Goldstein [2] performed experimental and numerical studies to determine velocity and temperature distributions and local heat transfer coefficients for convective flows of air ($Pr \approx 0.7$) and water ($Pr \approx 6$). Powe et al. [3, 4] and Rao et al. [5] investigated flow patterns for air. They found that the free convective flow of air can be categorized into four basic types: a steady two-dimensional flow with two crescent-shaped eddies, a two-dimensional oscillatory flow, a three-dimensional spiral flow, and a two-dimensional multicellular flow. Recently, Yoo [6] investigated the existence of dual steady states for a fluid of $Pr = 0.7$.

Thermal convection of fluids with low Prandtl number such as liquid metals exhibits more complicated flow patterns for high Rayleigh numbers [7–11]. Mack and Bishop [7] and Custer and Shaughnessy [8] investigated steady two-dimensional convection of a low Prandtl number fluid ($Pr = 0.02$) in a wide annulus with $D_i/L = 2$. They used a regular perturbation expansion in powers of Ra (or Gr and Pr) to obtain solutions for the streamfunction and temperature fields and found a steady multicellular flow composed of two weak eddies located in the top and bottom regions of annulus and a larger dominant eddy which rotates in the opposite sense. On the other hand, Charrier-Mojtabi et al. [9] considered unsteady two-dimensional equations. For $D_i/L = 2$ and $Pr = 0.02$, they observed oscillatory flows with two and three like-rotating cells in the half of an annulus. In particular, Fant et al. [10] studied unsteady natural convection for the limiting case of $Pr = 0$. They simplified the Boussinesq approximated Navier–Stokes equations to Cartesian-like boundary layer equations by means of a high Rayleigh number small-gap asymptotic expansion. They found that a steady multicellular instability sets in first, and then time-periodic and complex unsteady multicellular flows develop as the scaled gap spacing increases. Yoo et al. [11] investigated the unsteady natural convection of a fluid with $Pr = 0.02$. They observed steady and oscillatory multicellular flow patterns, and plotted the transition Grashof number at which the types of flow patterns were altered as functions of inverse relative gap width.

Some other authors considered a non-uniformly heated annular fluid layer [12], transient convection [13, 14], the condition of a constant heat flux at the inner cylinder [15], a conjugate problem [16], cold water [17], and an annulus with a rotating cylinder [18].

Up to date, most works for the natural convection in horizontal annuli have been performed for wide-gap annuli. Relatively few studies, however, have been made for narrow annuli. In particular, a systematic investigation on the effect of Prandtl number has not been made.

On the other hand, the natural convection problems in a vertical slot [19–22] and in a tall vertical annulus [23, 24] have been studied extensively. Korpela et al. [19] and Korpela [20] studied the stability of natural convection base flow in narrow, vertical, and inclined slots. They found that the value of Pr has the dominant influence upon the type of instability of the conduction-dominated flow. For the inclined slot geometry, only a hydrodynamic type of instability can occur for $Pr < 0.24$ [20]. Lee and Korpela [21] numerically studied the multicellular natural convection in a vertical slot, and supported the earlier results for the vertical slot [19].

A narrow horizontal annulus with a heated inner cylinder is an interesting physical system, since hydrodynamic instability can occur in the vertical section [21] and Rayleigh–Bénard thermal instability [25] can occur on the top part of thermally unstable region. We can imagine that very interesting natural convection phenomena must occur, and, of course, the Prandtl number is thought to play an important role.

In a horizontal annulus with a heated inner cylinder, there is no state in which the fluid is motionless. The conduction regime of natural convection for low values of Gr forms a crescent-shaped eddy in which fluid rises near the inner hotter cylinder and sinks near the outer colder one (Fig. 1). Walton [26] studied the stability of conduction regime of natural convection in a horizontal annulus by using a WKB formulation. He found that $Pr = 0.24$ was also a critical value of Prandtl number for the annular geometry. For $Pr > 0.24$, instability sets in at the top of cylinders ($\phi = 0$). For $Pr < 0.24$, the instability can first form elsewhere. The value of Pr is seen to play a fundamental role in characterizing the instability of conduction regime in narrow horizontal annulus.

The objective of the present study is to investigate the Prandtl number dependent natural convection in a narrow horizontal annulus. The unsteady Boussinesq approximated Navier–Stokes equations are numerically solved for an annulus with $D_i/L = 12$. It is found that the stability of the conduction regime of natural convection in a narrow horizontal annulus can be divided into the following two regimes:

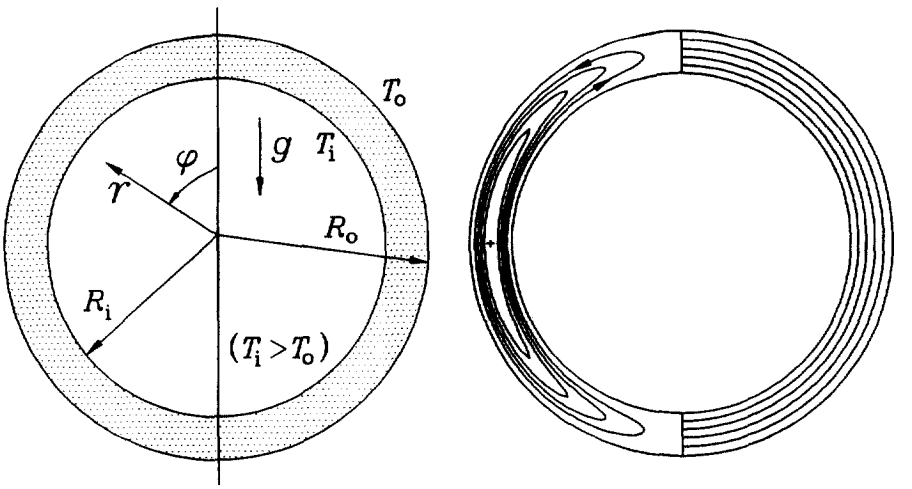

Fig. 1. A sketch of an annulus and a plot of streamlines and isotherms of conduction-dominated regime.

(1) For $Pr \leqslant 0.2$, the instability sets in as steady or oscillatory flows consisting of multiple like-rotating cells in the vertical section of annulus. The instability is hydrodynamic in its origin. The critical Grashof number is increased as Pr is decreased, and tends to a finite limit as $Pr \to 0$.

(2) For $Pr \geqslant 0.3$, the instability first sets in at the top portion of annulus, indicating that the instability is thermal in its origin. For $Pr = 0.3$, a square-shaped counter-rotating cell is formed on the top of annulus.

After the onset of instability of conduction regime, very complex oscillatory multicellular convection is developed, which is dependent on Pr. In this report the results for $Pr \leqslant 0.2$ and $Pr = 0.3$ are presented. And the results for $Pr \geqslant 0.4$ will be presented in the subsequent paper. The main features for $Pr \leqslant 0.2$ and $Pr = 0.3$ are as follows:

(1) $Pr \leqslant 0.2$: For $Pr \approx 0$, the like-rotating cells are distributed uniformly in the upper and the lower parts of annulus. As Pr is increased, however, the cells are shifted upwards. The multicellular flow pattern is observed to drift downward, and the speed of travel increases as Pr is increased.

(2) $Pr = 0.3$: As Gr is increased, the steady secondary flow with a counter-rotating cell on the top undergoes hydrodynamic instability. For $Pr = 0.3$, hydrodynamic and thermal instabilities are coexistent, and the oscillatory flows after secondary instability consist of multiple like-rotating cells in the vertical section of annulus and one or more counter-rotating cells on the top part. The shape and strength of the cells on the top are nearly unvarying, although the like-rotating cells in the vertical section undergo strong oscillatory motions. Multiple oscillatory flows characterized by the number of the cells on the top are found.

2. Analysis

The configuration to be studied and the coordinate system are seen in Fig. 1. The fluid is contained between two infinite horizontal concentric circular cylinders, which are held at different uniform temperatures of T_i and T_o ($T_i > T_o$). The thermophysical properties of fluid except density are assumed constant. And the Boussinesq approximation is employed such that the variation of density with temperature can be neglected except for the buoyancy force terms. The viscous dissipation in the energy equation is also neglected. We consider a two-dimensional problem, and use the cylindrical coordinates (r, ϕ), the angular coordinate ϕ being measured counter-clockwise from the upward vertical through the center of the cylinders (Fig. 1). The equations governing conservation of mass, momentum, and energy are put into non-dimensional form by taking the characteristic length, time, velocity, pressure, and temperature as L, L^2/ν, $V = \alpha g(T_i - T_o)L^2/\nu$, $\rho_0 V^2$, and $(T_i - T_o)$, respectively. We let $Pr = \nu/\chi$ and $Gr = \alpha g(T_i - T_o)L^3/\nu^2$ denote the Prandtl and Grashof numbers, respectively. The dimensionless governing equations are

$$\nabla \cdot \vec{u} = 0 \tag{1}$$

$$\frac{\partial \vec{u}}{\partial t} + Gr(\vec{u} \cdot \nabla)\vec{u} = -Gr\nabla p + \nabla^2 \vec{u} + \theta[\cos(\phi)\vec{e}_r - \sin(\phi)\vec{e}_\phi] \tag{2}$$

$$\frac{\partial \theta}{\partial t} + Gr(\vec{u} \cdot \nabla)\theta = \frac{1}{Pr}\nabla^2 \theta \tag{3}$$

with the boundary conditions

$$u = v = 0, \quad \theta = 1 \quad \text{at } r = r_i \tag{4}$$

$$u = v = 0, \quad \theta = 0 \quad \text{at } r = r_o \tag{5}$$

On the introduction of the streamfunction Ψ, continuity equation (1) is satisfied identically. And the dimensionless equations governing the two-dimensional convection in terms of the vorticity ω and streamfunction Ψ are written as follows:

$$\frac{\partial \omega}{\partial t} = GrJ(\Psi, \omega) + \nabla^2 \omega - \left[\sin(\phi) \frac{\partial \theta}{\partial r} + \cos(\phi) \frac{\partial \theta}{r \partial \phi} \right] \tag{6}$$

$$\omega = -\nabla^2 \Psi \tag{7}$$

$$\frac{\partial \theta}{\partial t} = GrJ(\Psi, \theta) + \frac{1}{Pr} \nabla^2 \theta \tag{8}$$

where the vorticity ω, streamfunction Ψ, Jacobian $J(f, g)$, and Laplacian ∇^2 are

$$\omega = \frac{\partial}{r \partial r}(rv) - \frac{\partial}{r \partial \phi}(u), \quad u = \frac{\partial \Psi}{r \partial \phi}, \quad v = -\frac{\partial \Psi}{\partial r}$$

$$J(f, g) = \frac{1}{r}\left(\frac{\partial f}{\partial r}\frac{\partial g}{\partial \phi} - \frac{\partial f}{\partial \phi}\frac{\partial g}{\partial r} \right)$$

$$\nabla^2 = \frac{\partial}{r \partial r}\left(r \frac{\partial}{\partial r} \right) + \frac{\partial^2}{r^2 \partial \phi^2} \tag{9}$$

The boundary conditions on the two walls are

$$\Psi = \frac{\partial \Psi}{\partial r} = 0, \quad \omega = -\frac{\partial^2 \Psi}{\partial r^2}, \quad \theta = 1 \quad \text{at } r = r_i \tag{10}$$

$$\Psi = \frac{\partial \Psi}{\partial r} = 0, \quad \omega = -\frac{\partial^2 \Psi}{\partial r^2}, \quad \theta = 0 \quad \text{at } r = r_o \tag{11}$$

We impose the following symmetric conditions

$$\Psi = \omega = \frac{\partial^2 \Psi}{\partial \phi^2} = \frac{\partial \theta}{\partial \phi} = 0 \quad \text{at } \phi = 0, \pi \tag{12}$$

since we suppose the flow to be symmetric with respect to the vertical plane through the center of cylinders.

The dimensionless heat transfer rate of pure conduction in the absence of fluid motion is

$$Nu_{cond} = \frac{1}{\ln(r_o/r_i)} \tag{13}$$

The local Nusselt number is defined as the actual heat flux divided by Nu_{cond}.

$$Nu_i(\phi) = -\left(r \frac{\partial \theta}{\partial r} \right) / Nu_{cond} \quad \text{at } r = r_i \tag{14}$$

$$Nu_o(\phi) = -\left(r \frac{\partial \theta}{\partial r} \right) / Nu_{cond} \quad \text{at } r = r_o \tag{15}$$

And the mean Nusselt numbers, $\overline{Nu_i}$ and $\overline{Nu_o}$, are given by

$$\overline{Nu_i} = \frac{1}{\pi} \int_0^{\pi} Nu_i(\phi)\, d\phi \tag{16}$$

$$\overline{Nu_o} = \frac{1}{\pi} \int_0^{\pi} Nu_o(\phi)\, d\phi \tag{17}$$

Equations (6)–(12) are numerically solved by using finite difference method. Equations (6) and (8) are cast into finite difference form using the leap-frog method [27] of Dufort–Frankel for the diffusion and time derivative terms, and central differencing for the Jacobian. The Poisson equation for the streamfunction is descretized by use of five-point formula. Because the computational domain is rectangular, the discretized Poisson equation is solved by the direct method of Buzbee et al. [28] which uses cyclic even–odd reduction method. The algorithm of Buzbee et al. [28] is known to be extremely fast and accurate. In the azimuthal direction, a uniform grid is employed, and in the radial direction, the following coordinate stretching is utilized.

$$r = r_i + \frac{1}{2}\left[1 + \frac{\tanh\{C(2\eta - 1)\}}{\tanh(C)} \right]$$

$$\text{with } C = 1.5, \quad 0 \leqslant \eta \leqslant 1 \tag{18}$$

This study uses the $(r \times \phi)$ meshes of (15×257) or (25×129). In the transitional regime of conduction-dominated flow, especially many grid points are used in the ϕ-direction to capture the weak initial instability occurring near the critical Grashof number. The time step Δt was taken in the range of $10^{-5} \leqslant \Delta t \leqslant 10^{-3}$. The accuracy of the numerical method was checked by Yoo [6].

To investigate the oscillatory flow, we record the following time variation of the radial velocity at the center of annular gap during the computational period:

$$u(t) = u(r_c, \pi/2, t) \quad \text{where } r_c = (r_i + r_o)/2 \tag{19}$$

Since hydrodynamic instability occurs in the vertical section of annulus, the point of $(r_c, \pi/2)$ is chosen. For a low-Prandtl number fluid, oscillatory multicellular flow occurs, and we record $N(t)$ defined as follows:

$$N(t) = \text{number of points } \phi \text{ at which}$$

$$u(r_c, \phi -, t) > 0 \quad \text{and} \quad u(r_c, \phi +, t) < 0 \tag{20}$$

$N(t)$ represents the number of points at which the sign of the instantaneous radial velocity at the centerline of annular gap $(r_c, 0 < \phi < \pi)$ is changed over from plus to minus, starting from $\phi = 0$. For small Pr and Gr, the streamlines of the multicellular flow are smooth, and $N(t)$ is equal to the instantaneous number of cells rotating counter-clockwise direction.

We record $u(t)$ to see the temporal behavior of velocity field, and $N(t)$ is recorded to measure the complexity of

the instantaneous spatial structure of oscillatory flow field.

3. Results and discussion

Computations were performed for various combinations of Pr and Gr with $D_i/L = 12$ in the range of $0.001 \leqslant Pr \leqslant 0.3$ and $Gr \leqslant 5 \times 10^4$. We consider half of an annulus, since the flow is assumed symmetric with respect to the vertical plane through the center of cylinders. It was found that the stability of the conduction regime of natural convection in a narrow horizontal annulus for $Pr \leqslant 0.2$ and $Pr = 0.3$ has the following characteristics.

(1) For $Pr \leqslant 0.2$, the instability sets in as steady or oscillatory flows consisting of multiple like-rotating cells in the vertical section of annulus.

(2) For $Pr = 0.3$, the instability sets in as a steady flow with one counter-rotating cell on the top of annulus.

The location at which the instability of conduction regime occurs is in accordance with the result of Walton [26].

The results are presented in two subsections of [$Pr \leqslant 0.2$] and [$Pr = 0.3$], according to the type of the instability of conduction regime.

3.1. [Pr $\leqslant$ 0.2]

In this range of Prandtl number, two kinds of transition phenomena were observed: (i) For $Pr \leqslant 0.01$, steady one-cell flow of conduction regime → steady flow with two like-rotating cells → oscillatory flow with multiple like-rotating cells; (ii) For $0.02 \leqslant Pr \leqslant 0.2$, steady one-cell flow of conduction regime → oscillatory flow consisting of multiple like-rotating cells.

The map of flow regimes on the Pr–Gr plane is plotted in Fig. 2. The critical Grashof number at which the instability of conduction regime occurs is increased as Pr is decreased, and tends to a finite limit as $Pr \to 0$. This study obtained $Gr_c \approx 8900$ with $Pr = 0.001$, which is larger than the value of $Gr_c \approx 7932$ for a vertical slot with $Pr = 0$ [19]. For $Pr = 0.2$, the results of Walton [26] give $Gr_c \approx 7369$ with $D_i/L = 12$. This study obtained $Gr_c \approx 7300$ for $Pr = 0.2$ (Fig. 2). The value of the present study is close to that of Walton, but is slightly smaller. The difference may be caused by the small-gap approximation made by Walton. His results are accurate for $L/D_i \to 0$, and give $Gr_c \approx 7020$ for $L/D_i = 0$. The above results imply that Gr_c is decreased as L/D_i decreases. For very small Prandtl number ($Pr = 0.001$), the region in which instability of conduction regime first forms is near $\phi = \pi/2$, but is extended upward with increase of Pr. For all values of $Pr \leqslant 0.2$, however, all the cells rotate in the same direction. We can conclude that a transition from steady one-cell (or multiple like-rotating-cell) flow to oscillatory multicellular flow occurs in the range of $Pr \leqslant 0.2$. The streamline pattern of the steady two like-rotating cells for $Pr \leqslant 0.01$ is similar to that in Fig. 4(b): at the initial stage of instability, the secondary cell formed in the upper region of annulus is very weak, but we can see the formation of the cell clearly with the help of the radial velocity distribution.

The diagram of Fig. 2 was obtained with the $(r \times \phi)$ mesh of (15×257). Especially many grid points were used in the ϕ-direction to capture the weak initial instability occurring near the critical Grashof number. The meshes of (15×129) or (25×129) also yielded qualitatively identical results, although the transitional Grashof numbers were about 3% higher than those obtained with (15×257) mesh. The oscillatory convection after the onset of instability has been investigated with (25×129) mesh: a test of grid-dependency was made with $Pr = 0.01$ and $Gr = 10^4$, and it was observed that the meshes of (25×129), (15×257), or (25×257) yielded identical results.

After the onset of oscillatory convection, the spatial structure of the flow becomes increasingly complex and the number of like-rotating cells is sequentially increased, as Gr is increased. One representative value of Pr is taken as $Pr = 0.01$, and the oscillatory behavior of $N(t)$ and $u(t)$ is presented in Fig. 3 with $Gr = 8900$, 9000, 10^4, and 1.5×10^4. For $Pr = 0.01$, the convection is steady, up to $Gr = 8800$. But oscillatory convection occurs at $Gr = 8900$. Figure 3 presents the transient behavior of $N(t)$ and $u(t)$ after sudden heating of inner cylinder. For the values of Gr in Fig. 3, the flows are smooth, and $N(t)$ is equal to the number of cells rotating counter-clockwise direction. The figure shows that $N(t)$ experiences an oscillatory motion of 1–2–1–2–1–2–3–2–3 when Gr is close to Gr_c ($Gr = 8900$), but for $Gr \geqslant 9000$ $N(t)$ increases stepwise, after impulsive heating of cylinder. And afterwards, successive 4–5, 4–5, 5–6, and 7–8 cellular patterns occur periodically, for $Gr = 8900$, 9000, 10^4, and 1.5×10^4, respectively. The 4, 5, and 6 cellular patterns of $Gr = 8900$, 9000 and 10^4 are similar to those in Fig. 4(d)–(f). And the 7–8 cellular patterns of $Gr = 1.5 \times 10^4$ are shown in Fig. 5. The above shows that the initial instability formed in the vertical region near $\phi = \pi/2$ propagates along the circumference of annulus, and the number of like-rotating cells is sequentially increased, as Gr is increased.

The onset and propagation of instability after impulsive heating of cylinder are illustrated in Fig. 4 with $Pr = 0.01$ and $Gr = 10^4$. The initial conditions are $\vec{u} = \theta = 0$, and the inner cylinder is suddenly heated to $\theta = 1$. After a second, a pseudo-conduction state with a crescent-shaped cell is established (a). The velocity profile at this stage is approximated $u(r_c, 0) \cos(\phi)$. As time goes on, however, hydrodynamic instability occurs near the vertical portion of annulus ($\phi = \pi/2$), and the radial velocity profile is increasingly skewed (b–f). During the tran-

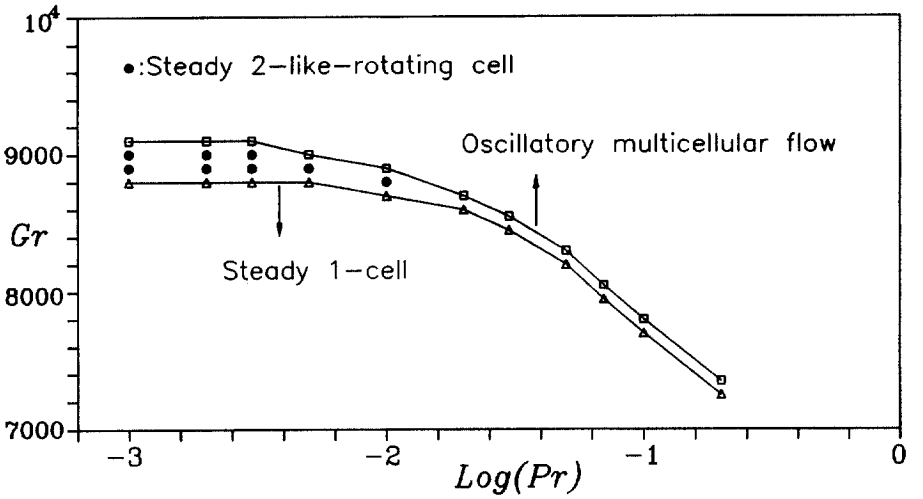

Fig. 2. Stability diagram Pr vs Gr. '●' represents a steady flow with two like-rotating cells in the vertical section of annulus.

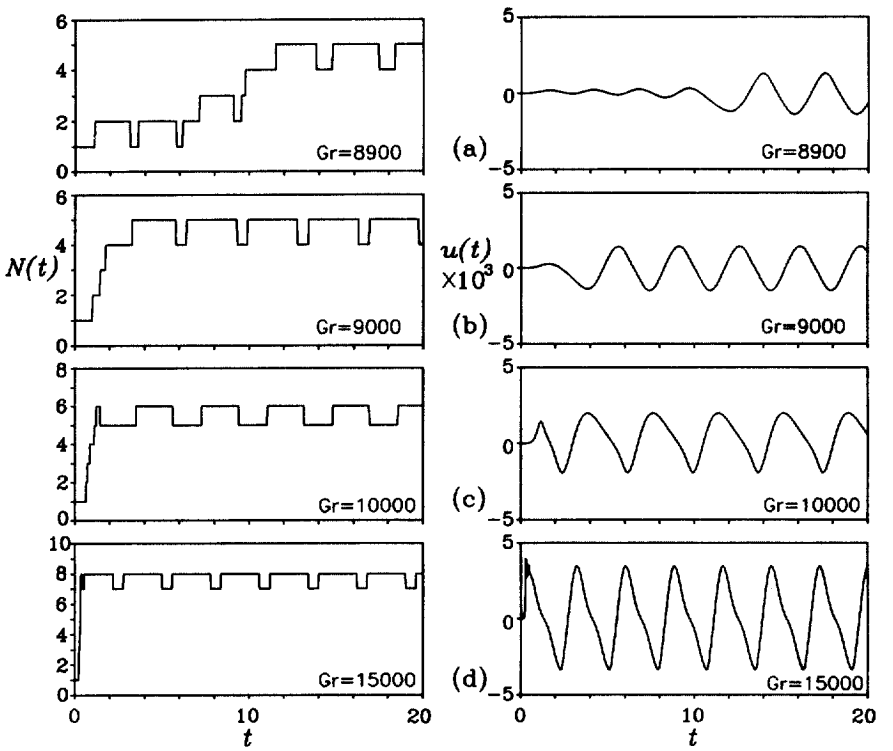

Fig. 3. Time evolution of $N(t)$ and $u(t)$ for several Grashof numbers with $Pr = 0.01$: (a) $Gr = 8900$; (b) $Gr = 9000$; (c) $Gr = 10^4$; (d) $Gr = 1.5 \times 10^4$. The initial conditions are $\vec{u} = \theta = 0$, and the inner cylinder is suddenly heated to $\theta = 1$. For the parameters of the present figure, $N(t)$ is equal to the number of cells rotating counter-clockwise direction.

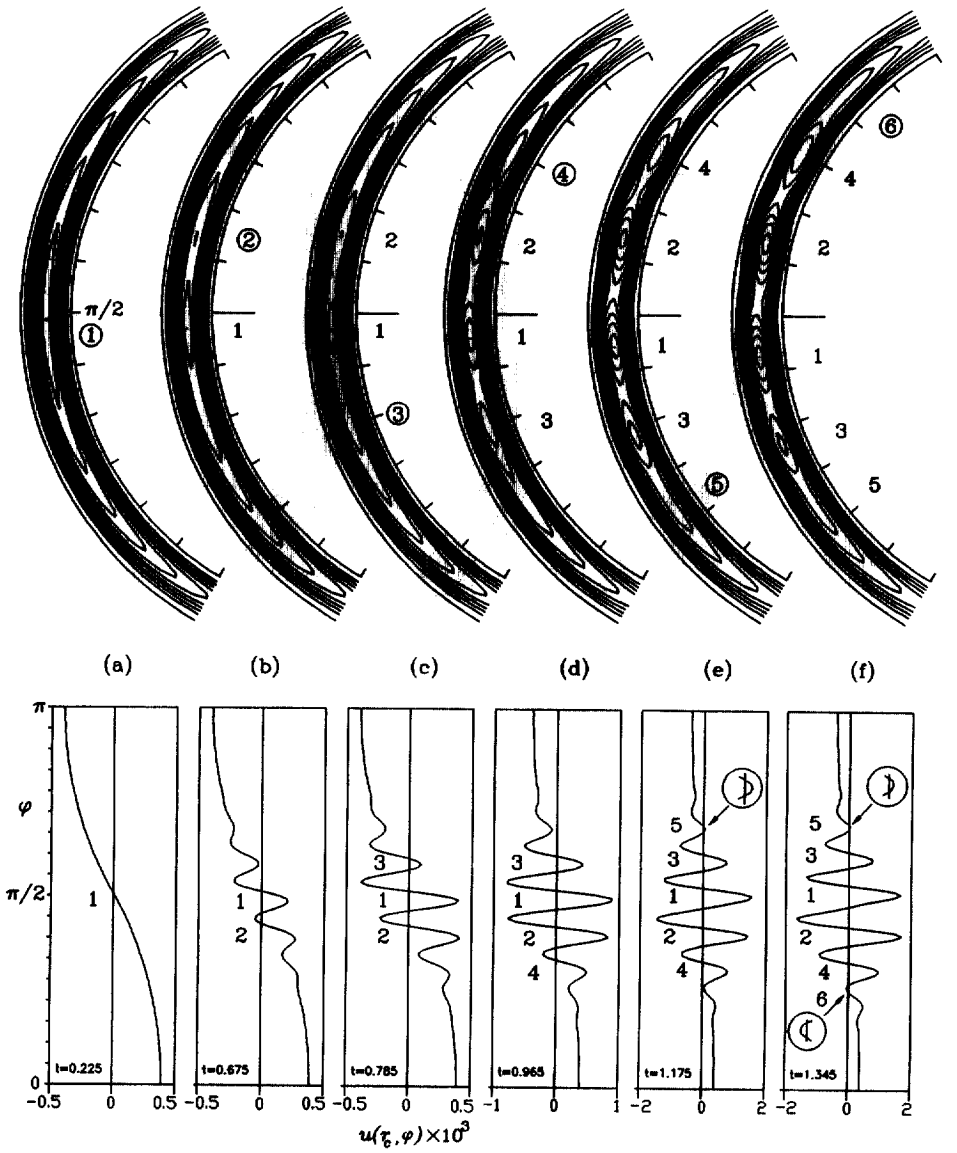

Fig. 4. A transient development of flow pattern and distribution of radial velocity at the centerline of annular gap, $u(r_c, \phi)$, with $Gr = 10^4$ and $Pr = 0.01$: at (a) $t = 0.225$; (b) $t = 0.675$; (c) $t = 0.785$; (d) $t = 0.965$; (e) $t = 1.175$; (f) $t = 1.345$. The initial conditions are $\vec{u} = \theta = 0$, and the inner cylinder is suddenly heated to $\theta = 1$.

sient period, the strongest cell in the vicinity of $\phi = \pi/2$ (cell 1) drifts downward, as time goes on. And new cells which rotate counter-clockwise direction are created alternately in the upper ($\phi < \pi/2$) and the lower ($\phi > \pi/2$) regions of annulus (b–f). The velocity profiles and streamline patterns of Fig. 4 well show the onset and propagation of instability for small Pr.

An example of the periodic motion of the cells is shown in Fig. 5 with $Gr = 1.5 \times 10^4$ and $Pr = 0.01$. The fluctuation of $u(t)$ is presented in Fig. 3(d). At $t = t_1$, at which $u(t)$ takes its minimum value, seven cells are visible in Fig. 5(a). The flow in each cell rotates counter-clockwise. As time goes on, all the cells drift downward, and a new cell is created in the space of the top portion of the chain of cells (Fig. 5(b)). The strength of a cell is increased as it approaches the vertical portion of annulus ($\phi = \pi/2$). Afterwards, however, the strength slowly diminishes and by the time they reach the bottom portion of annulus, the cell has vanished. The motion of cells in Fig. 5 is in accordance with the results of Yoo et al. [11], but is

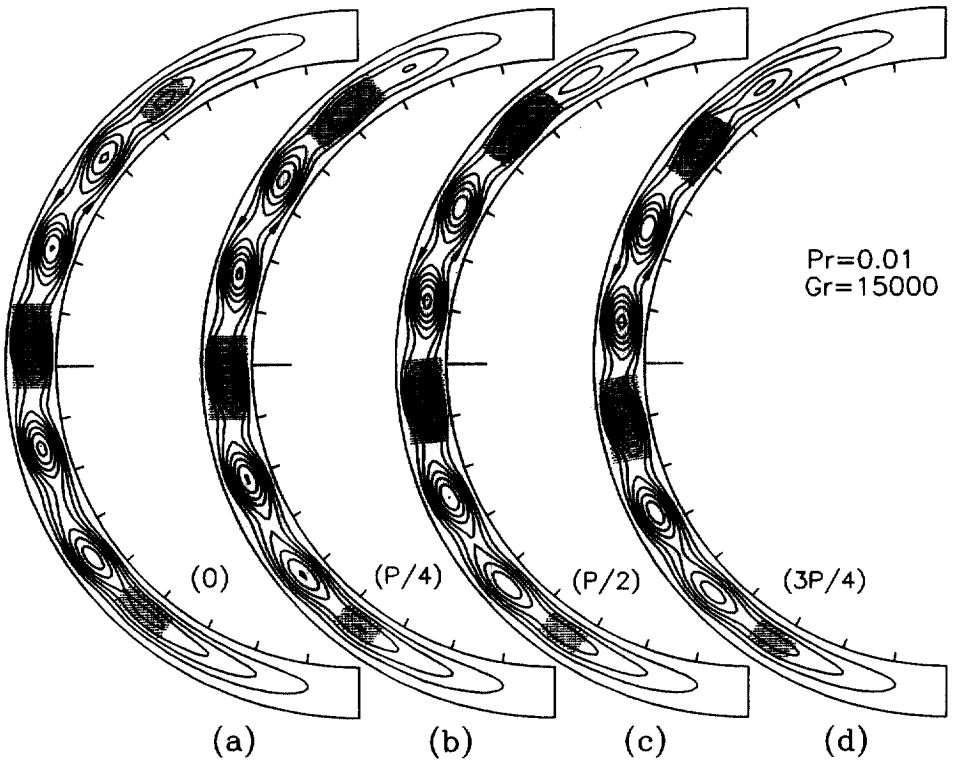

Fig. 5. Instantaneous streamlines over one period of oscillation for $Gr = 1.5 \times 10^4$ and $Pr = 0.01$: (a) at $t = t_1$ at which $u(t)$ takes its minimum value; (b) at $t = t_1 + P/4$; (c) at $t = t_1 + P/2$; (d) at $t = t_1 + 3P/4$. Three structures are shaded with dots so that their motion can be followed.

different from those of Fant et al. [10] in which the oscillatory motion is composed of coalescence and separation of cells in the vicinity of $\phi = \pi/2$. The difference may be caused by their simplified governing equations which neglect azimuthal diffusion. The phenomenon of the drifting of cells along the circumference of cylinder can be compared with the case of a vertical annulus with heated inner cylinder, in which multicellular flow pattern is observed to drift upward [23, 24]. During the oscillation period, the strongest cell is near the vertical portion of annulus ($\phi = \pi/2$), and it is different from the case of a vertical slot in which the strongest cells are in the ends of the slot [21].

The influence of Pr on the oscillatory behavior is shown in Fig. 6 with $Gr = 10^4$. The periodic flows are composed of successive 5–6, 6–7, and 5–6–7 cellular patterns for $Pr \leqslant 0.02$ (a, b), $Pr = 0.1$ (c), and $Pr = 0.2$ (d), respectively. The period of oscillation for $Gr = 10^4$ and 2×10^4 as functions of Pr is presented in Fig. 7. The figure shows that the period is decreased, as Pr or Gr is increased. The general trend observed is that the oscillatory motion occurs fast and the spatial structure of flow becomes complex, as Pr or Gr is increased.

The effect of Pr on the spatial structure of flow is shown in Fig. 8. The figure presents the instantaneous streamlines for $Pr = 0.001$, 0.05, 0.1, and 0.2 with $Gr = 2 \times 10^4$. For very small Pr, the multiple cells are distributed uniformly in the lower and upper regions of annulus (a). As Pr is increased, however, the cells are shifted upwards (b). At $Pr = 0.1$ (c), five cells are clearly visible in the upper region of $\phi < \pi/2$, but only two cells in the lower region of $\phi > \pi/2$. The strength of a cell in the top portion of the chain of cells becomes strong, as Pr is increased (c). At $Pr = 0.2$ (d), a new counter-rotating cell is formed on the top of annulus during the oscillation period. In all cases of Fig. 8, the multicellular flow pattern is observed to drift downward, and the speed of travel increases as Pr is increased (Fig. 7).

For $Pr = 0.2$, the counter-rotating cell on the top of annulus is also observed at $Gr = 10^4$, in which the cell appears and disappears periodically. At $Gr = 2 \times 10^4$, however, the cell does not disappear during the oscillation period, and an oscillatory multicellular flow which shows different behavior from the case of $Pr = 0.01$ (Fig. 5) is observed. The temporal behavior of flow patterns for $Pr = 0.2$ and $Gr = 2 \times 10^4$ is presented in Fig. 9. The main features of the flow can be described as follows. As the cell in the top of the chain of like-rotating cells, 'cell

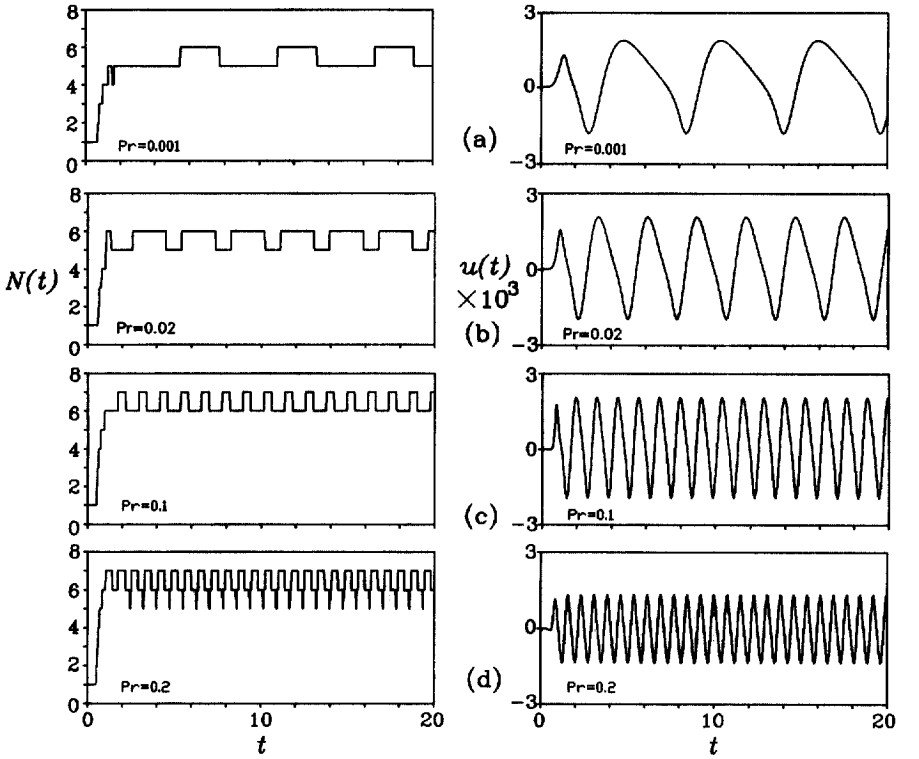

Fig. 6. Time evolution of $N(t)$ and $u(t)$ for several Prandtl numbers with $Gr = 10^4$: (a) $Pr = 0.001$; (b) $Pr = 0.02$; (c) $Pr = 0.1$; (d) $Pr = 0.2$. The initial conditions are $\vec{u} = \theta = 0$, and the inner cylinder is suddenly heated to $\theta = 1$.

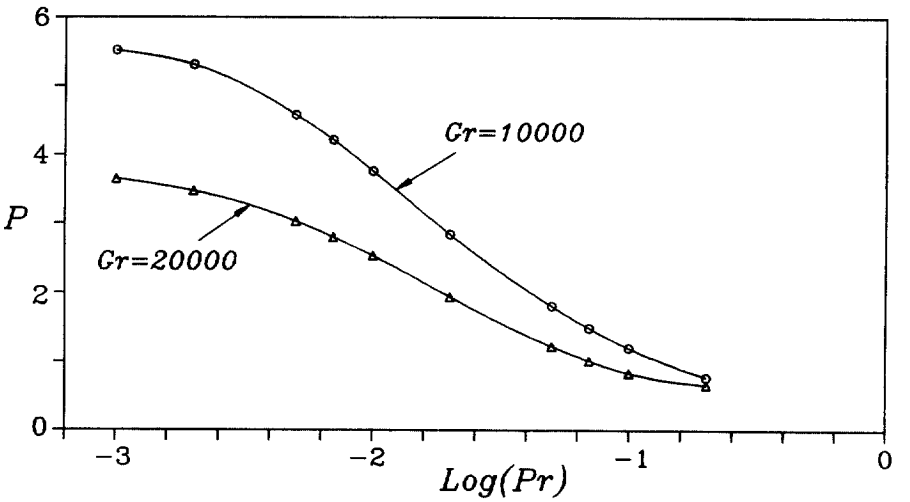

Fig. 7. Period of oscillation (P) as function of Prandtl number for $Gr = 10^4$ and 2×10^4.

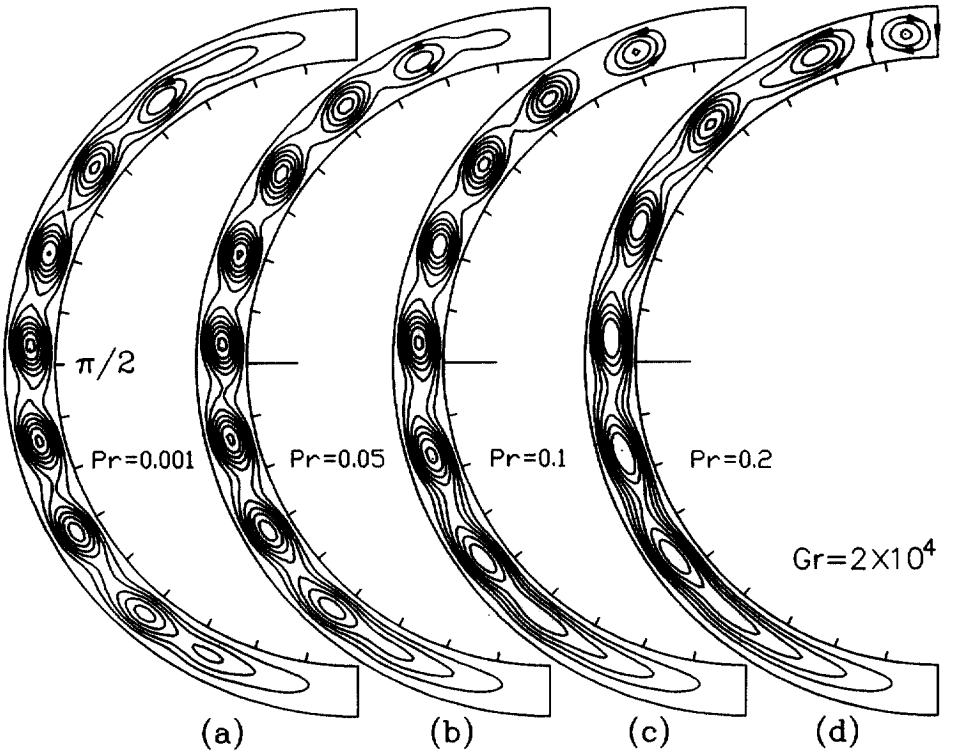

Fig. 8. Effect of Prandtl number on convection with $Gr = 2 \times 10^4$: (a) $Pr = 0.001$; (b) $Pr = 0.05$; (c) $Pr = 0.1$; (d) $Pr = 0.2$. For each value of Pr, the fluctuation of $u(t)$ shows simple periodic motion which is similar to those in Fig. 6, and the plotted is the instantaneous streamlines at $t = t_1$, at which $u(t)$ takes its minimum value.

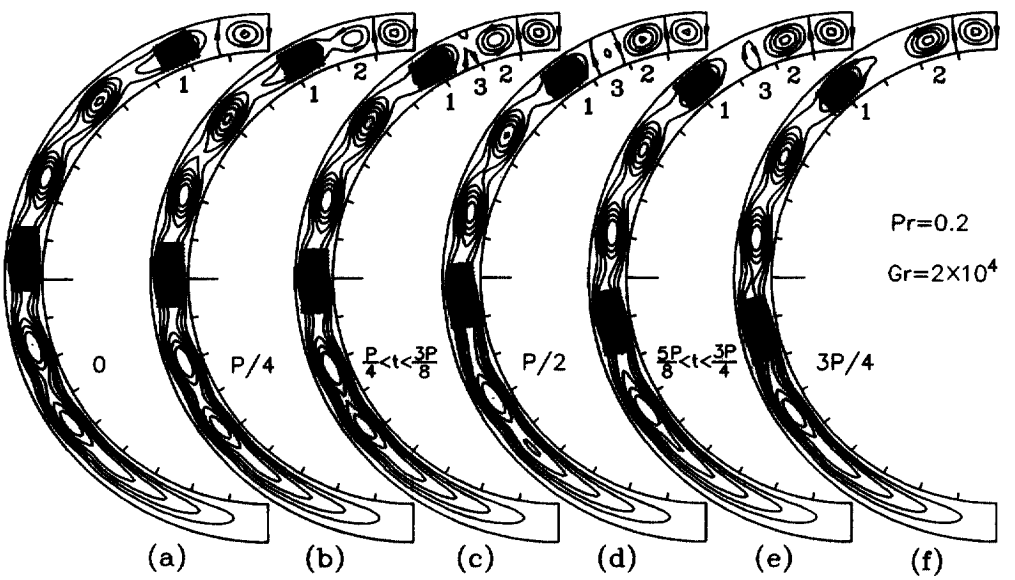

Fig. 9. Time sequence of streamfunction field over one period of oscillation for $Pr = 0.2$ and $Gr = 2 \times 10^4$: (a) at $t = t_1$ at which $u(t)$ takes its minimum value; (b) at $t = t_1 + P/4$; (c) at $t_1 + P/4 < t < t_1 + 3P/8$; (d) at $t = t_1 + P/2$; (e) at $t_1 + 5P/8 < t < t_1 + 3P/4$; (f) at $t = t_1 + 3P/4$. Two structures are shaded with dots so that their motion can be followed.

1', drifts downward (a), the space between the counter-rotating cell and 'cell 1' becomes wide, and a new cell, 'cell 2', is created in that space, and grows in size (b). Next, as 'cell 1' drifts further downward, the viscous drag of 'cell 1' and 'cell 2' creates a new counter-rotating cell, 'cell 3', between the two cells (c, d). As 'cell 1' drifts further downward, however, 'cell 3' becomes weak, and finally disappears (e, f). Afterwards, 'cell 2' in (f) drifts downward, and plays the role of 'cell 1' in (a). And one cycle of the periodic motion is completed. During the period, the counter-rotating cell on the top of annulus is contracting and expanding in size.

For relatively small Gr near Gr_c, the region occupied by the multiple cells is narrow, and the cells are slim (Fig. 4). As Gr increases, the number of the like-rotating cells is increased, and the region occupied by the cells is extended over the whole annulus at high Gr (Fig. 8). Diagrams of flow patterns for $Pr = 0.01$ and 0.1 are presented in Fig. 10, in which $N(t)$ represents the complexity of the spatial structure of oscillatory multicellular flow. For relatively

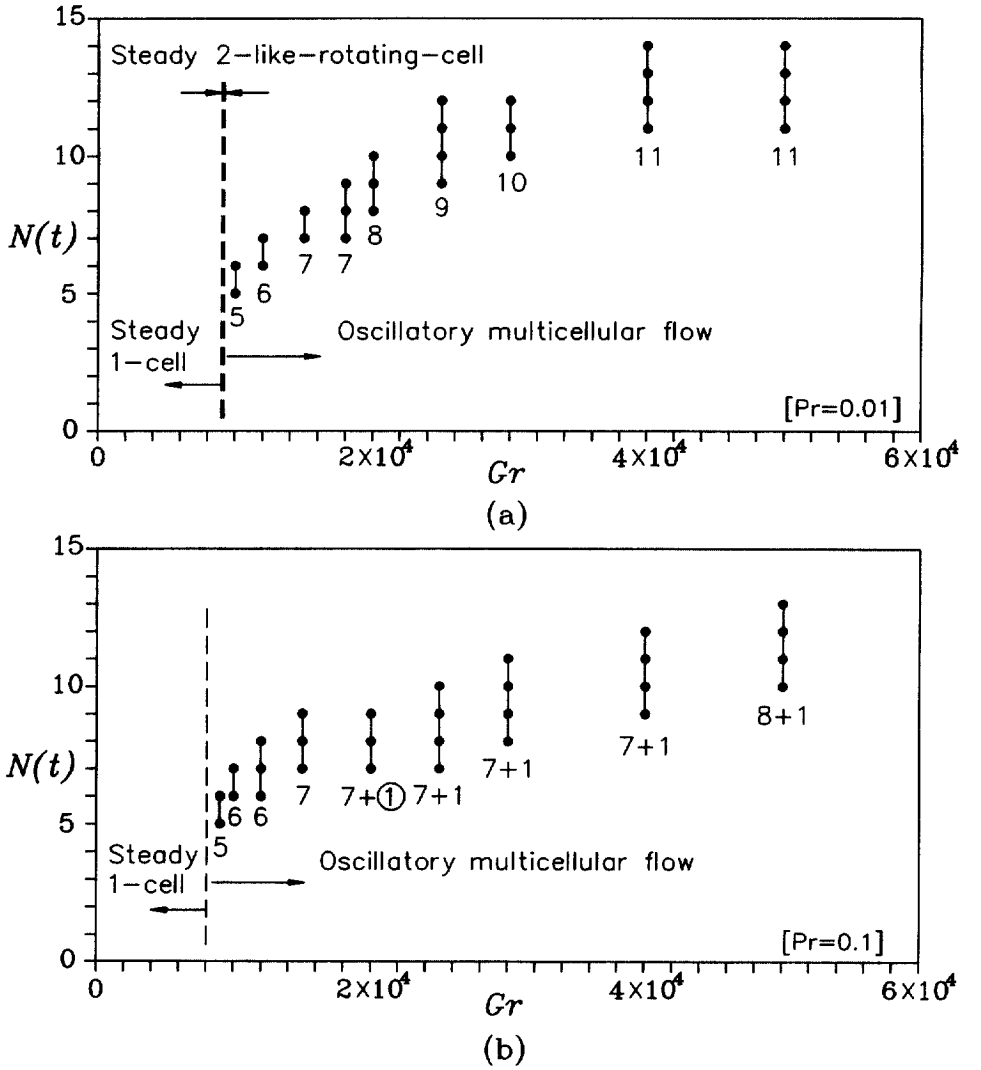

Fig. 10. Diagrams of flow patterns for $Pr = 0.01$ (a) and 0.1 (b). The numbers in the figure represent the number of like-rotating cells which are clearly visible during the oscillation period, at each Gr. In (b), '7 + 1' (or '8 + 1') represents seven (or eight) like-rotating cells plus one counter-rotating cell on the top of annulus. And '+①' at $Gr = 2 \times 10^4$ represents that the counter-rotating cell on the top appears and disappears periodically.

small Gr, $Gr \leqslant 1.5 \times 10^4$ for $Pr = 0.01$ and $Gr \leqslant 10^4$ for $Pr = 0.1$, the flow is smooth and $N(t)$ is equal to the number of cells rotating counter-clockwise direction. For $Pr = 0.01$, sequential increase of the number of like-rotating cells can be seen as Gr is increased, which demonstrates the smooth propagation of the initial instability set in near $\phi = \pi/2$ along the circumference of cylinder. As Pr increases, the influence of thermal instability in the upper region of annulus becomes strong. For $Pr = 0.1$, a counter-rotating cell appears on the top of annulus at $Gr \geqslant 2 \times 10^4$.

3.2. [Pr = 0.3]

For a fluid with $Pr = 0.3$, the conduction-dominated flow is maintained up to $Gr = 6000$, but the flow becomes unstable with increase of Gr, and finally a new flow pattern with a counter-rotating cell on the top of annulus is established at $Gr = 7000$. The steady-state streamlines at $Gr = 7000$ and the distributions of radial velocities at $Gr = 6000$ and 7000 are presented in Fig. 11. We can see that the streamlines and the velocity profile of $Gr = 7000$ are nearly identical to those of the conduction regime except the region of $0 < \phi < 30°$. The top part of an annulus with a heated inner cylinder is thermally unstable. And the above results show that the first instability for $Pr = 0.3$ is thermal in its origin. It is to be noted that the value of $Ra = 2100$, corresponding to $Gr = 7000$ and $Pr = 0.3$, is not much larger than the critical Rayleigh number of $Ra_c = 1708$ in the Rayleigh–Bénard convection [25].

As Gr is increased further, the steady secondary flow with a counter-rotating cell undergoes an oscillatory instability at $Gr \geqslant 8000$. The transient mean Nusselt numbers and time evolutions of $u(t)$ for $Gr = 8000$, 1.2×10^4, 2×10^4, and 3×10^4 are presented in Fig. 12. At the initial stage of oscillatory instability ($Gr = 8000$), the unsteady motion is periodic in time and shows fluctuations of constant amplitude. The fluctuation becomes fast with increase of Gr, and apparently chaotic motions are developed at $Gr = 2 \times 10^4$ and 3×10^4. A few instantaneous streamlines and isotherms are presented in Fig. 13. The figure shows multiple like-rotating cells in the vertical section of annulus and one or more counter-rotating cells on the top part. It was observed that the cells separated by the streamline of $\Psi = 0$ on the top did not disappear during the oscillation period. The like-rotating cells in the vertical section undergo strong oscil-

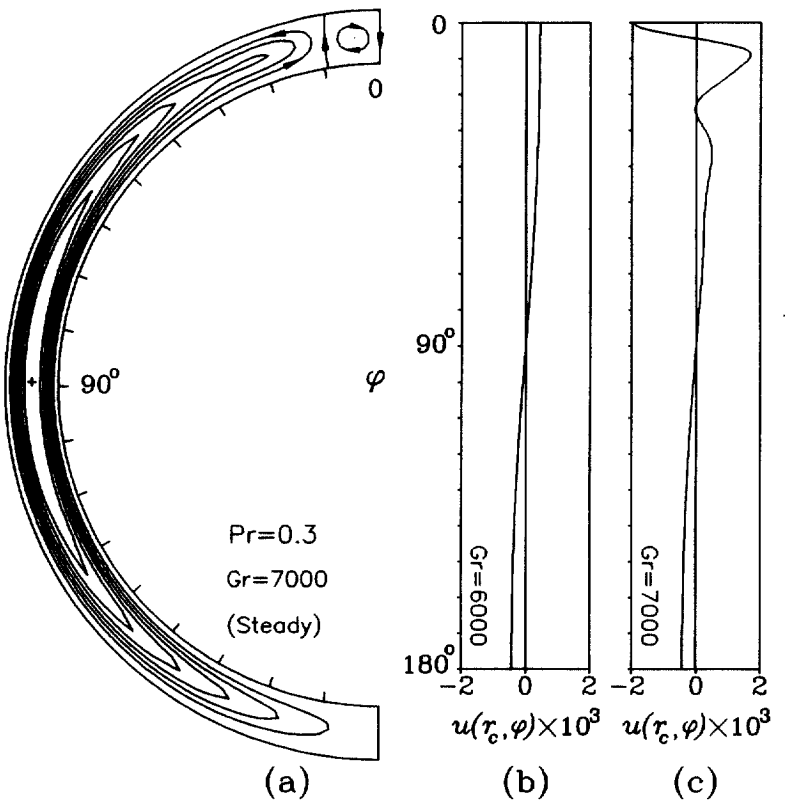

Fig. 11. Steady-state streamlines and variation of radial velocity at the centerline of annular gap, $u(r_c, \phi)$, for $Pr = 0.3$: (a) streamlines at $Gr = 7000$; (b) radial velocity at $Gr = 6000$; (c) radial velocity at $Gr = 7000$.

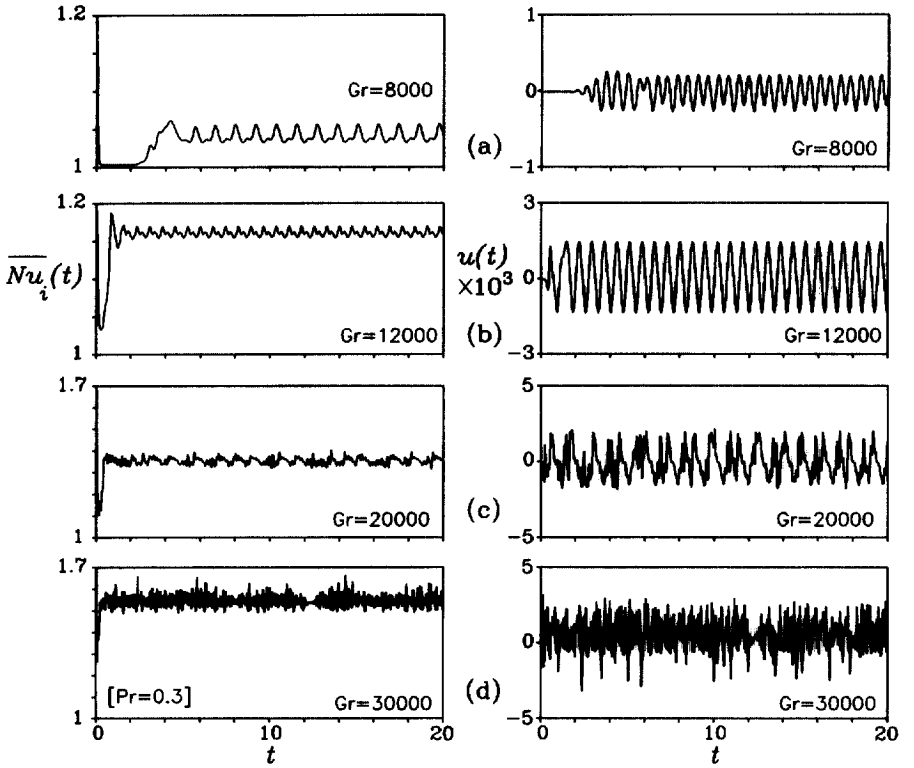

Fig. 12. Transient mean Nusselt number at the inner cylinder and time evolution of $u(t)$ for several Grashof numbers with $Pr = 0.3$: (a) $Gr = 8000$; (b) $Gr = 1.2 \times 10^4$; (c) $Gr = 2 \times 10^4$; (d) $Gr = 3 \times 10^4$.

latory motions; nevertheless, the shape and strength of the cells on the top are nearly unvarying for all time. The above indicates that the secondary oscillatory instability after the first instability is hydrodynamic in its nature, although the first instability of conduction regime at $Gr = 7000$ is thermal in its origin.

Figure 13 shows one, two, three, and four square-shaped cells on the upper part of annulus for $Gr = 8000$, 1.2×10^4, 2×10^4, and 3×10^4, respectively. The general trend observed is that as Gr is increased, the number of the cells and the size of the region occupied by the cells are increased. If we start the computation from zero initial condition, solutions with one and four cells are usually obtained for $Gr = 10^4$ and 5×10^4, respectively. It was observed, however, that the number of the cells were dependent on the initial condition or time step used in the computation. For example, when Gr was increased to 1.2×10^4 starting from an instantaneous solution obtained for $Gr = 8000$ with one cell on the top (Fig. 13a) as the initial condition, a time-periodic flow with one square-shaped cell on the top was established. The above implies that multiple oscillatory flows which can be distinguished by the number of cells in the thermally unstable region of annulus can occur for $Pr = 0.3$. The phenomena can be compared with the previous study of Yoo [6], in which dual steady solutions for air ($Pr = 0.7$) were investigated. For $Pr = 0.7$, steady-state convections with two type of cells were found [6]. But for $Pr = 0.3$, hydrodynamic instability occurring in the vertical section of annulus makes the system unsteady, and multiple oscillatory flows can be developed.

To investigate the above phenomena systematically, Gr was increased starting from $Gr = 6000$, and the solution was found by letting the initial condition be the instantaneous solution previously obtained (up-scan). And starting from the instantaneous solution of $Gr = 5 \times 10^4$ with four cells on the upper part of annulus as initial condition, the Gr was then sequentially decreased (down-scan). The results are presented in Fig. 14. In the figure, $N_{(\text{cells on top})}$ represents the number of square-shaped cells on the upper part of annulus. We can see transitions from one to three cells at the up-scan stage, and from four to two cells at the down-scan stage. It has also been tried to find hysteresis phenomenon, and the phenomenon was observed between the solution branches of $N_{(\text{cells on top})} = 2$ and 4 at high Gr. When the number of cells on the top is odd, the fluid in the central plane of annulus ($\phi = 0$) descends (Fig. 13(a), (c)), and when the number is even, the fluid ascends (Fig. 13(b), (d)). The temperature gradient between the inner and outer cyl-

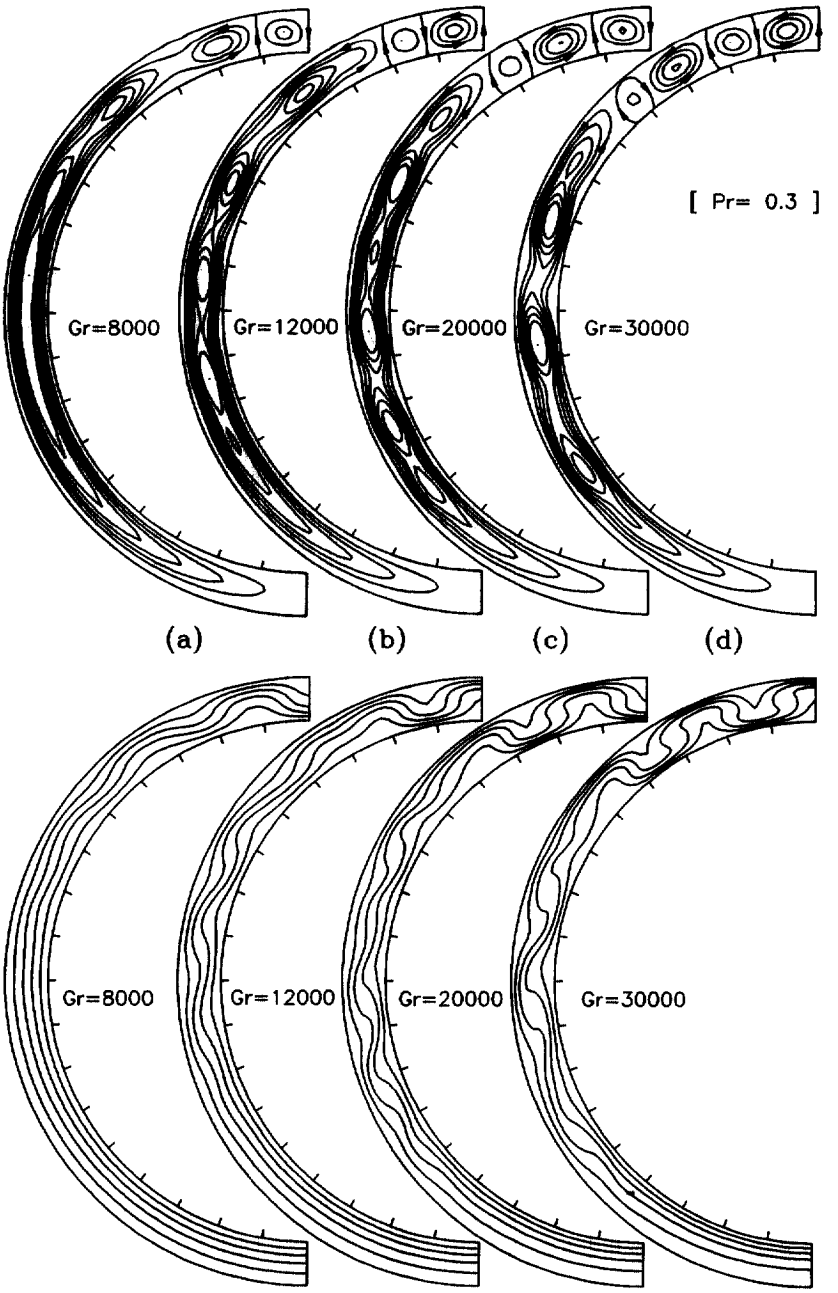

Fig. 13. Instantaneous streamlines and isotherms for $Pr = 0.3$: (a) $Gr = 8000$; (b) $Gr = 1.2 \times 10^4$; (c) $Gr = 2 \times 10^4$; (d) $Gr = 3 \times 10^4$.

inders in the vertical direction is the greatest at $\phi = 0$. The transitions imply that once the thermal plume at the plane of $\phi = 0$ has been established (directed downward or upward), its direction is not varied by the increase or decrease of Gr, after the onset of secondary instability ($Gr \geqslant 8000$). Figure 14 shows that multiple oscillatory flows characterized by the number of cells in the thermally unstable region of annulus can occur at $Gr \geqslant 8000$.

It is to be noted, however, that only a steady flow with a counter-rotating cell on the top occurs at the onset of the first instability of conduction regime at $Gr = 7000$, regardless of initial conditions. The flow is periodic in time for $Gr \leqslant 1.5 \times 10^4$, but is apparently nonperiodic for $Gr \geqslant 2 \times 10^4$. The oscillatory motion can be classified in further detail, such as periodic motion with subharmonic frequency, quasi-periodic with two or three incom-

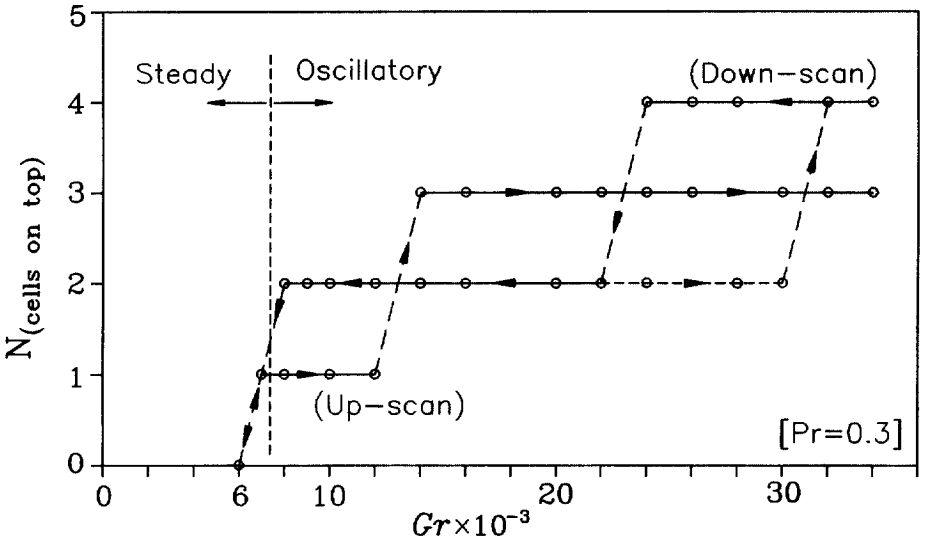

Fig. 14. Diagram showing the solution branches found for $Pr = 0.3$: $N_{(\text{cells on top})}$ represents the number of square-shaped cells separated by the streamline of $\Psi = 0$ on the upper part of annulus.

mensurable frequencies, etc. This study has focused the main attention on the spatial structure of the convective flows. The route to temporal chaos is also an interesting subject [29, 30], and that for the natural convection in a horizontal annulus remains to be studied.

Although multiple steady solutions for several hydrodynamic problems (Taylor problem, Dean problem etc.) have been investigated experimentally and theoretically [30–34], the existence of multiple oscillatory flows has never been reported in any of the numerical and/or experimental studies as far as the present author is aware. For a narrow annulus with a heated cylinder, multiple oscillatory flows can occur, since hydrodynamic and thermal instabilities are coexistent in the fluid with an intermediate value of Pr ($Pr = 0.3$). That is, the thermal instability can yield multiple flows and the hydrodynamic instability can induce oscillatory flows.

An example of dual oscillatory flows is shown in Fig. 15 with $Gr = 1.4 \times 10^4$ having two or three cells on the top of annulus. It can be clearly seen that the like-rotating cells in the vertical section of annulus drift downward as time goes on, but the two (or three) cells on the top are almost unvarying. This is due to the stabilizing effect of viscous force and temperature field in the thermally unstable region, that is once the thermal plume on the top has been established, the viscous force maintains the shape of thermal plume at high Pr. In the case of (II), the strength of the counter-rotating cell interfaced with the end of the chain of like-rotating cells is very weak, but the cell persists for all time. It is different from the case of relatively low Pr, $Pr = 0.2$ (Fig. 9), in which the cells on the top appear and disappear periodically, and the counter-rotating cell is contracting and expanding in size.

The temporal development of cells after impulsive heating of cylinder is shown in Fig. 16 with $Gr = 2 \times 10^4$. The initial conditions are $\vec{u} = \theta = 0$, and the inner cylinder is suddenly heated to $\theta = 1$. After a second, a pseudo-conduction state with a crescent-shaped cell is established (a). And afterwards instability occurs in the vertical section of annulus, creating like-rotating cells (b). As time goes on, the instability propagates upward (c, d), and the strength of the cell on the top of the chain of cells becomes strong (e). And finally, the increased strength of the cell creates a counter-rotating cell on the top of annulus (f, g). As time goes on further, all the cells except the cell on the top of the chain of cells drift downward, and a new counter-rotating cell is formed (h), and grows in size (i, j). The plot of transient Nusselt number shows that $\overline{Nu}_i(t)$ is increased during the time interval of about $0.15 \leqslant t \leqslant 0.45$ during which the pseudo-conduction state having been broken and the cells are created sequentially. After the formation of the three cells on the top ($t > 0.45$), however, $\overline{Nu}(t)$ ceases to increase but fluctuates. We can see that the cellular convection increases the heat transfer at wall.

As a final observation on the effect of Gr and flow pattern, their influence on heat transfer is shown in Fig. 17. The figure presents the time-averaged overall Nusselt number ($\overline{Nu}_{\text{time}}$) as functions of Gr. From the figure, we can see relatively steep increase in the overall Nusselt number when the number of the square-shaped cells on the upper part of annulus is increased from one to three

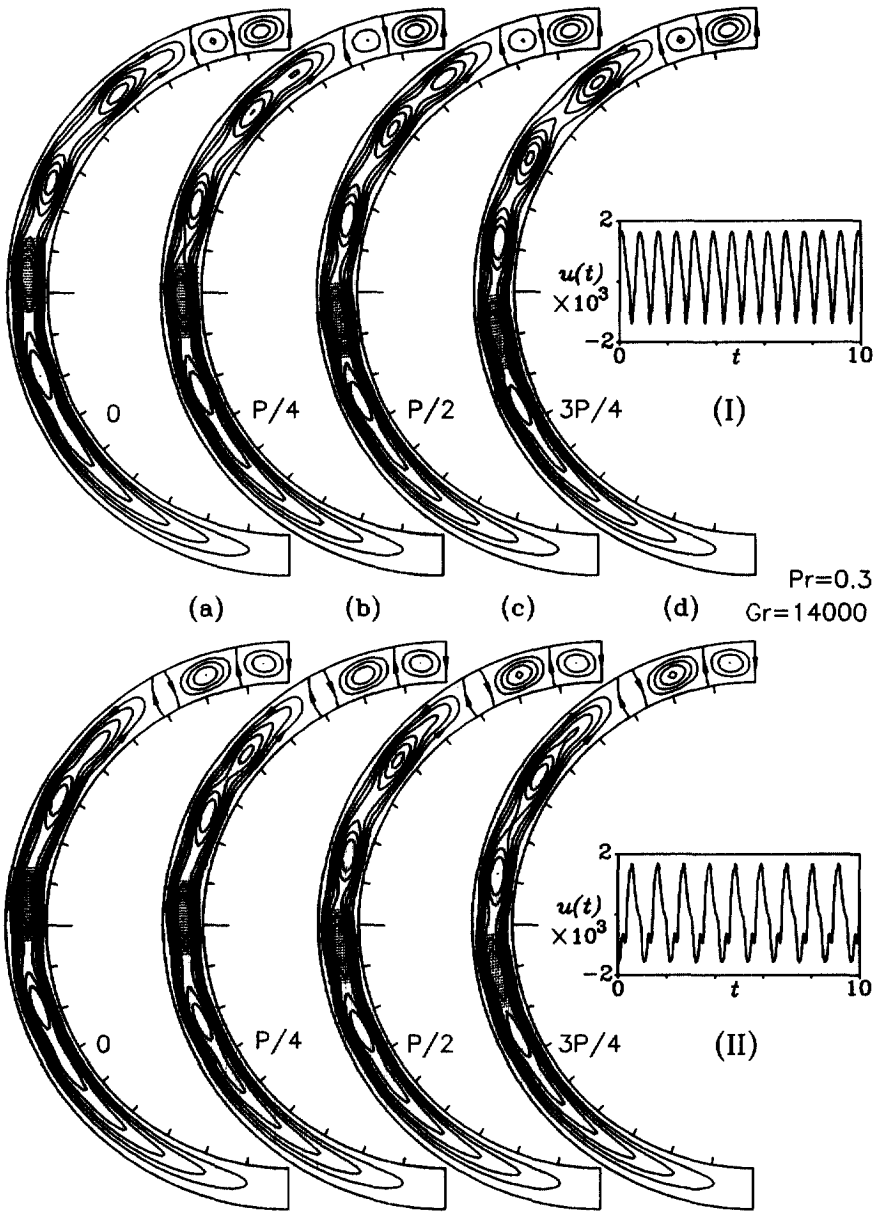

Fig. 15. Plots of $u(t)$ and time sequence of instantaneous streamlines over one period of oscillation for $Pr = 0.3$ and $Gr = 1.4 \times 10^4$ having flows with two (I) and three (II) cells on the top of annulus: (a) at $t = t_1$ at which $u(t)$ takes its minimum value; (b) at $t = t_1 + P/4$; (c) at $t = t_1 + P/2$; (d) at $t = t_1 + 3P/4$. One structure is shaded with dots so that its motion can be followed.

(or from two to four), at the up-scan stage. And at the down-scan stage, relatively steep decrease in Nu_{time} can be seen when the number of the cells is decreased from four to two. In the regime of multiple oscillatory flows, the flow with the more cells on the top of annulus has the greater overall Nusselt number than the other flows. Cellular convection forms thermal plumes between the cells, and the heat transfer at the wall is increased with increase of the number of cells (or thermal plumes).

4. Conclusions

Natural convection in a narrow horizontal concentric annulus is numerically investigated. Unsteady two-dimen-

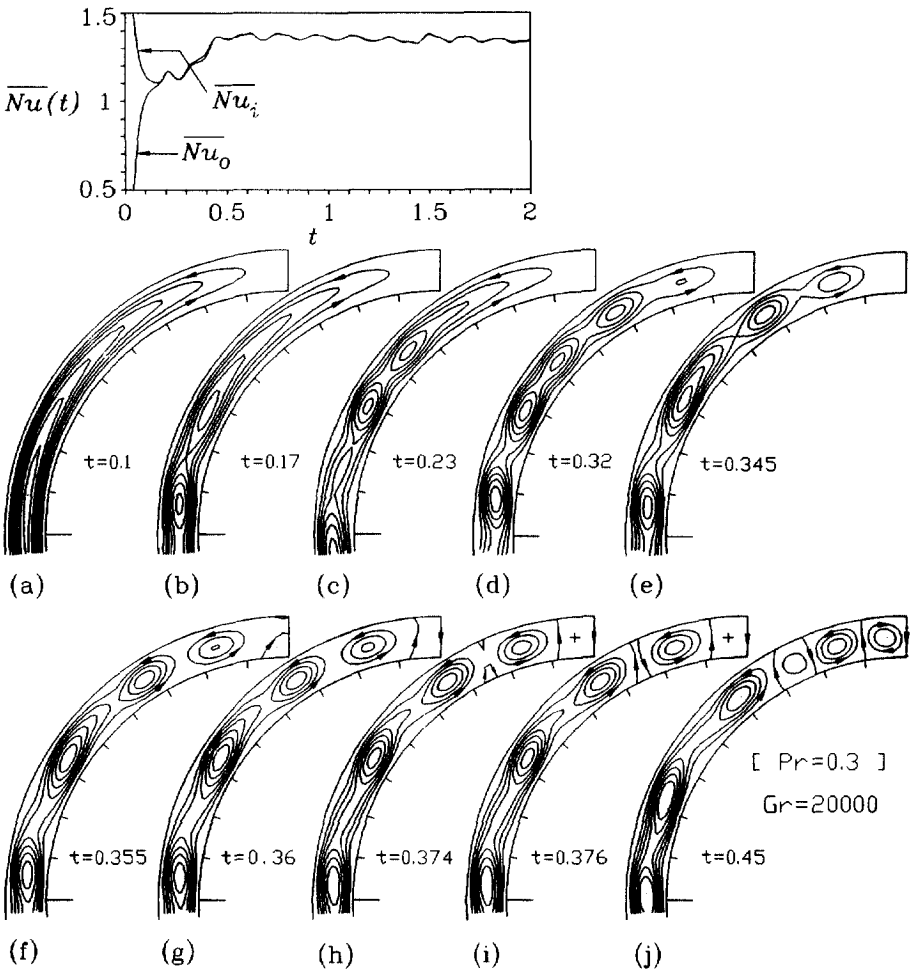

Fig. 16. Transient mean Nusselt numbers and development of the flow patterns for $Pr = 0.3$ and $Gr = 2 \times 10^4$: at (a) $t = 0.1$; (b) $t = 0.17$; (c) $t = 0.23$; (d) $t = 0.32$; (e) $t = 0.345$; (f) $t = 0.355$; (g) $t = 0.36$; (h) $t = 0.374$; (i) $t = 0.376$; (j) $t = 0.45$. The initial conditions are $\vec{u} = \theta = 0$, and the inner cylinder is suddenly heated to $\theta = 1$.

sional streamfunction–vorticity equation is solved by using finite difference method. It is found that the stability of the conduction regime of natural convection for $Pr \leqslant 0.2$ and $Pr = 0.3$ has the following characteristics: (1) For $Pr \leqslant 0.2$, hydrodynamic instability induces steady or oscillatory flows consisting of multiple like-rotating cells in the vertical section of annulus; (2) For $Pr = 0.3$, thermal instability creates one counter-rotating cell on the top of annulus. For $Pr \approx 0$, the region in which instability of conduction regime first forms is near $\phi = \pi/2$, but is extended upward with increase of Pr. After the onset of instability, diverse oscillatory multicellular convections are developed, according to Pr. For a fluid of $Pr \approx 0$, the multiple cells are distributed uniformly in the lower and upper regions of annulus. As Pr is increased, however, the cells are shifted upwards. The like-rotating cells drift downward, as time goes on, and the speed of travel increases as Pr is increased. For $Pr = 0.3$, hydrodynamic and thermal instabilities are coexistent, and the oscillatory flows after secondary instability consist of multiple like-rotating cells in the vertical section of annulus and one or more counter-rotating cells on the top part. It is observed that the shape and strength of the square-shaped cells on the top are almost unvarying, although the like-rotating cells in the vertical section undergo strong oscillatory motions. The oscillatory instability is hydrodynamic in nature. Multiple oscillatory flows characterized by the number of the cells on the top are found for $Pr = 0.3$. Time-averaged overall Nusselt number at the wall is increased with increase of the number of cells on the top.

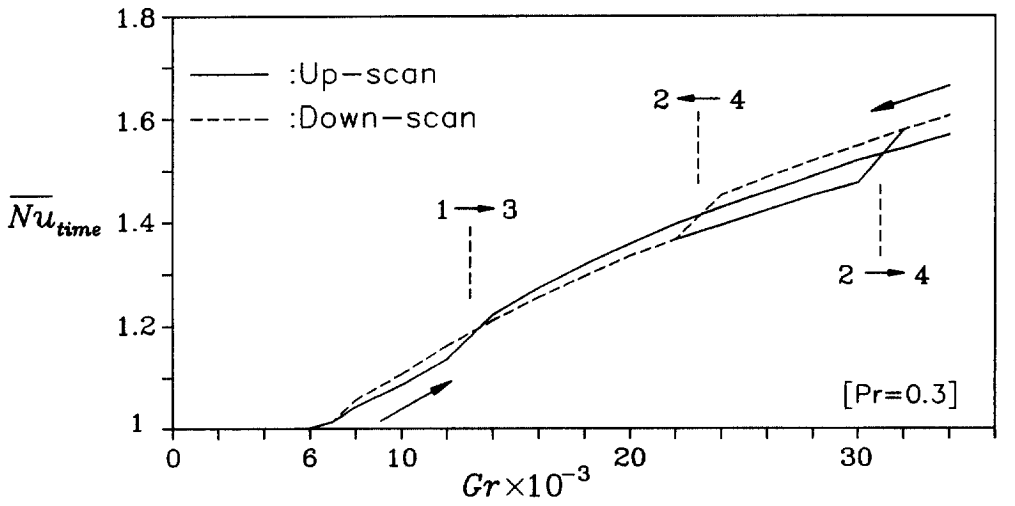

Fig. 17. Time-averaged overall Nusselt number ($\overline{Nu}_{time}$) for $Pr = 0.3$. In the non-periodic regime of Gr, integration is carried out from $t = t_B$ to $t = t_B + 20$, and the last part of data for $\overline{Nu}$ are averaged over the time interval of $\Delta t = 10$. Continuous and dashed lines represent the curves of $\overline{Nu}_{time}$ at the up-scan and down-scan stages, respectively. The symbols '1 → 3' and '2 ← 4' indicate the points (Gr) at which the number of cells separated by the streamline of $\psi = 0$ on the upper part of annulus is increased from one to three at the up-scan stage, and is decreased from four to two at the down-scan stage, respectively. The symbol '2 → 4' indicates the point (Gr) at which the number of cells is increased from two to four, with increase of Gr.

References

[1] Gebhart B, Jaluria Y, Mahajan RL, Sammakia B. Buoyancy-induced flows and transport. Hemisphere Publishing Corporation 1988;764–71.

[2] Kuehn TH, Goldstein RJ. An experimental and theoretical study of natural convection in the annulus between horizontal concentric cylinders. Journal of Fluid Mechanics 1976;74:695–719.

[3] Powe RE, Carley CT, Bishop EH. Free convective flow patterns in cylindrical annuli. Journal of Heat Transfer 1969;91:310–14.

[4] Powe RE, Carley CT, Carruth SL. A numerical solution for natural convection in cylindrical annuli. Journal of Heat Transfer 1971;93:210–20.

[5] Rao YF, Miki Y, Fukuda K, Takata Y, Hasegawa S. Flow patterns of natural convection in horizontal cylindrical annuli. International Journal of Heat and Mass Transfer 1985;28:705–14.

[6] Yoo J-S. Dual steady solutions in natural convection between horizontal concentric cylinders. International Journal of Heat and Fluid Flow 1996;17:587–93.

[7] Mack LR, Bishop EH. Natural convection between horizontal concentric cylinders for low Rayleigh numbers. Quarterly Journal of Mechanics and Applied Mathematics 1968;21:223–41.

[8] Custer JR, Shaughnessy EJ. Thermoconvective motion of low Prandtl number fluids within a horizontal cylindrical annulus. Journal of Heat Transfer 1977;99:596–602.

[9] Charrier-Mojtabi MC, Mojtabi A, Caltagirone JP. Numerical solution of a flow due to natural convection in horizontal cylindrical annulus. Journal of Heat Transfer 1979;101:171–73.

[10] Fant DB, Prusa J, Rothamayer AP. Unsteady multicellular natural convection in a narrow horizontal cylindrical annulus. Journal of Heat Transfer 1990;112:379–87.

[11] Yoo J-S, Choi J-Y, Kim M-U. Multicellular natural convection of a low Prandtl number fluid between horizontal concentric cylinders. Numerical Heat Transfer, Part A 1994;25:103–15.

[12] Prud'homme M, Robillard L, Vasseur P. A study of laminar natural convection in a nonuniformly heated annular fluid layer. International Journal of Heat and Mass Transfer 1987;30:1209–222.

[13] Tsui YT, Tremblay B. On transient natural convection heat transfer in the annulus between concentric horizontal cylinders with isothermal surfaces. International Journal of Heat and Mass Transfer 1984;27:103–11.

[14] Castrejon A, Spalding DB. An experimental and theoretical study of transient free-convection flow between horizontal concentric cylinders. International Journal of Heat and Mass Transfer 1988;31:273–84.

[15] Kumar P. Study of natural convection in horizontal annuli. International Journal of Heat and Mass Transfer 1988;31:1137–148.

[16] Kolesnikov PM, Bubnovich VI. Non-stationary conjugate free-convective heat transfer in horizontal cylindrical coaxial channels. International Journal of Heat and Mass Transfer 1988;31:1149–56.

[17] Ho CJ, Lin YH. Laminar natural convection of cold water enclosed in a horizontal annulus with mixed boundary conditions. International Journal of Heat and Mass Transfer 1998;31:2113–21.

[18] Yoo J-S. Mixed convection of air between two horizontal concentric cylinders with a cooled rotating outer cylinder. International Journal of Heat and Mass Transfer 1998;41:293–302.

[19] Korpela SA, Gozum D, Baxi CB. On the stability of the

conduction regime of natural convection in a vertical slot. International Journal of Heat and Mass Transfer 1973;16:1683–90.

[20] Korpela SA. A study on the effect of Prandtl number on the stability of the conduction regime of natural convection in an inclined slot. International Journal of Heat and Mass Transfer 1974;17:215–22.

[21] Lee Y, Korpela SA. Multicellular natural convection in a vertical slot. Journal of Fluid Mechanics 1983;126:91–121.

[22] Chait A, Korpela SA. The secondary flow and its stability for natural convection in a tall vertical enclosure. Journal of Fluid Mechanics 1989;200:189–216.

[23] Choi IG, Korpela SA. Stability of the conduction regime of natural convection in a tall vertical annulus. Journal of Fluid Mechanics 1980;99:725–38.

[24] Le Quéré P, Pécheux J. Numerical simulations of multiple flow transitions in axisymmetric annulus convection. Journal of Fluid Mechanics 1989;206:517–44.

[25] Busse FH. Transition to turbulence in Rayleigh–Bénard convection. In Topics in Applied Physics, Vol. 45, ed. HL Swinney and JP Gollub. Springer-Verlag, 1981. pp. 97–137.

[26] Walton IC. The stability of free convection in a horizontal cylindrical annulus. Quarterly Journal of Mechanics and Applied Mathematics 1980;33:125–39.

[27] Roache PJ. Computational fluid dynamics. Hermosa 1972;53–64.

[28] Buzbee BL, Golub GH, Nielson CW. On direct methods for solving Poisson's equations. SIAM Journal on Numerical Analysis 1970;7:627–56.

[29] Schuster HG. Deterministic Chaos. Physik-Verlag, 1984. pp. 31–136.

[30] Yoo J-S, Kim M-U. Two-dimensional convection in a horizontal fluid layer with spatially periodic boundary temperatures. Fluid Dynamics Research 1991;7:181–200.

[31] Zandbergen PJ, Dijkstra D, Von Kármán swirling flows. Annual Review of Fluid Mechanics 1987;19:465–91.

[32] Dennis SCR, Ng M. Dual solutions for steady laminar flow through a curved tube. Quarterly Journal of Mechanics and Applied Mathematics 1982;35:305–24.

[33] Benjamin TB, Mullin T. Notes on the multiplicity of flows in the Taylor experiment. Journal of Fluid Mechanics 1982;121:219–30.

[34] Nandakumar K, Masliyah JH, Law HS. Bifurcation in steady laminar mixed convection flow in horizontal ducts. Journal of Fluid Mechanics 1985;152:145–61.